

ANALYTICAL ELECTRON MICROSCOPY OF A CHONDRULE WITH RELICT OLIVINE IN THE ALH-77015 CHONDRITE (L3)

Seiko WATANABE, Masao KITAMURA and Nobuo MORIMOTO

*Department of Geology and Mineralogy, Faculty of Science,
Kyoto University, Sakyo-ku, Kyoto 606*

Abstract: Fine texture and chemical composition of relict olivines and pyroxenes in a chondrule in the ALH-77015(L3) chondrite have been studied by a transmission electron microscope with an analytical mode. Dusty cores of the relict olivines have abundant fine inclusions of chromite. In addition, they show dislocations extremely high in density with the predominant Burgers vector of [001]. The dislocations are considered to have been caused by shock impact.

Pyroxene grains in the same chondrule show an apparent crystallization sequence of the order of orthoenstatite, clinoenstatite and augite, which cannot be explained by a single crystallization stage. The orthoenstatite crystals are, therefore, considered to be relict.

1. Introduction

Chondrules have been considered to have rapidly cooled from melt. Either the melt was derived directly from condensation of the gas of the solar nebula or from the secondary melting of preexisting solid materials has been an attractive but unsolved problem. NAGAHARA (1981a) and RAMBALDI (1981) found many olivine grains with dusty cores and clear rims in the porphyritic chondrules in the unequilibrated ordinary chondrites. Reverse and normal zonings in Mg and Fe distribution were found in the dusty cores of several tens μm in size and the clear rims surrounding them, respectively. These results indicate that the crystallization processes of the dusty cores and clear rims are different and the dusty cores are relict crystals. These relict olivines, therefore, strongly support existence of olivine grains before melting in the formation process of chondrules.

Therefore, the study of the fine textures of the relict olivine is important to obtain information on the process during and before the formation of chondrules. Furthermore, the bulk composition of the chondrules cannot be explained only by olivine, suggesting existence of relict crystals other than olivine. In this study the chemical composition and fine texture of the relict olivine and the coexisting pyroxene grains in a chondrule in ALH-77015 (L3) have been examined by analytical electron microscopy (AEM).

2. Experimental and Result

ALH-77015 (L3) is a highly unequilibrated chondrite and has been precisely described by NAGAHARA (1981b) and FUJIMAKI *et al.* (1981). A great number of chondrules of various types and irregularly shaped fragments are inbedded in the dark

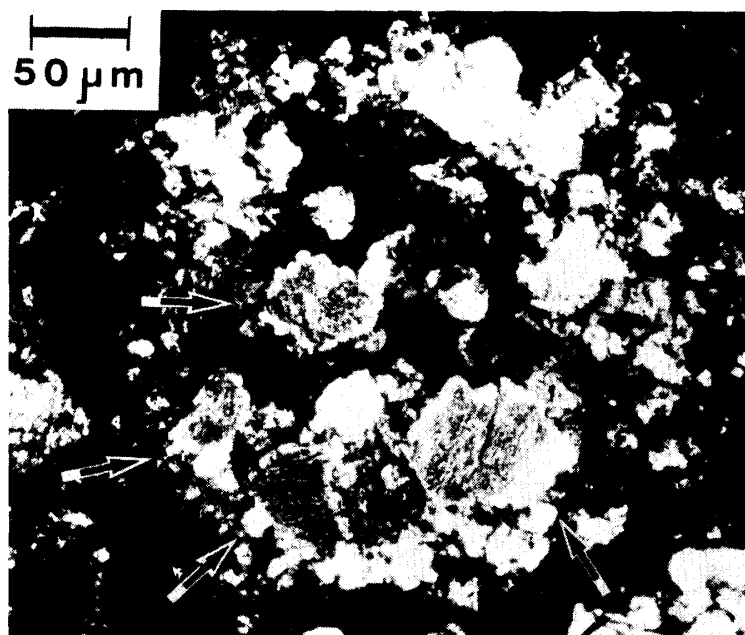


Fig. 1. Optical micrograph of chondrule. Relict olivine grains with dusty core and clear rim are indicated by arrows.

matrix.

Figure 1 is an optical micrograph of one of the chondrules. It is of somewhat irregular shape and about 0.3 mm in diameter, and consists mainly of olivine, pyroxene and opaque minerals. Some of olivine porphyries are large ($>50 \mu\text{m}$) and have the dusty core and narrow clear rim. Interstices among them and the opaque minerals are olivine and a minor amount of pyroxene of about $10 \mu\text{m}$ in size. Fine plagioclase was found by electron microscopy. This chondrule was ion-thinned and examined by a 200 kV transmission electron microscope (HITACHI-700H) with an analytical mode (AEM). The AEM analyses were carried out in the same manner as that described by MORIMOTO and KITAMURA (1981).

2.1. Olivine

In order to elucidate the zoning pattern of the dusty olivine, AEM analyses were carried out (see Appendix) by avoiding abundant fine inclusions in olivine, which will be described below. Since TEM observation was limited only to the small parts of the specimen thin enough to transmit the electrons, the path of analytical points is irregular and does not reach the center of the grain, as shown in the optical photomicrograph (Fig. 2a). At the outermost point of the rim, A in Fig. 2, the composition is Fa_{18} . As going into the grain, fayalite content decreases to the minimum of Fa_{11} at B, and then gradually increases up to Fa_{18} at C (Fig. 2b). The content is about Fa_{15} at points around D, and increases to Fa_{21} at the innermost point E.

Dusty appearance of the core of the olivine is due to inclusions of chromite (Fig. 3), though preferential ion-thinning results in holes around many of the chromite inclusions. Size and abundance of chromite inclusions are $0.1\text{--}0.2 \mu\text{m}$ and $1/\mu\text{m}^2$, respectively. AEM analytical result of a relatively large chromite, of which diffraction pattern is shown in Fig. 3, is given in Appendix. This value probably is not the real compo-

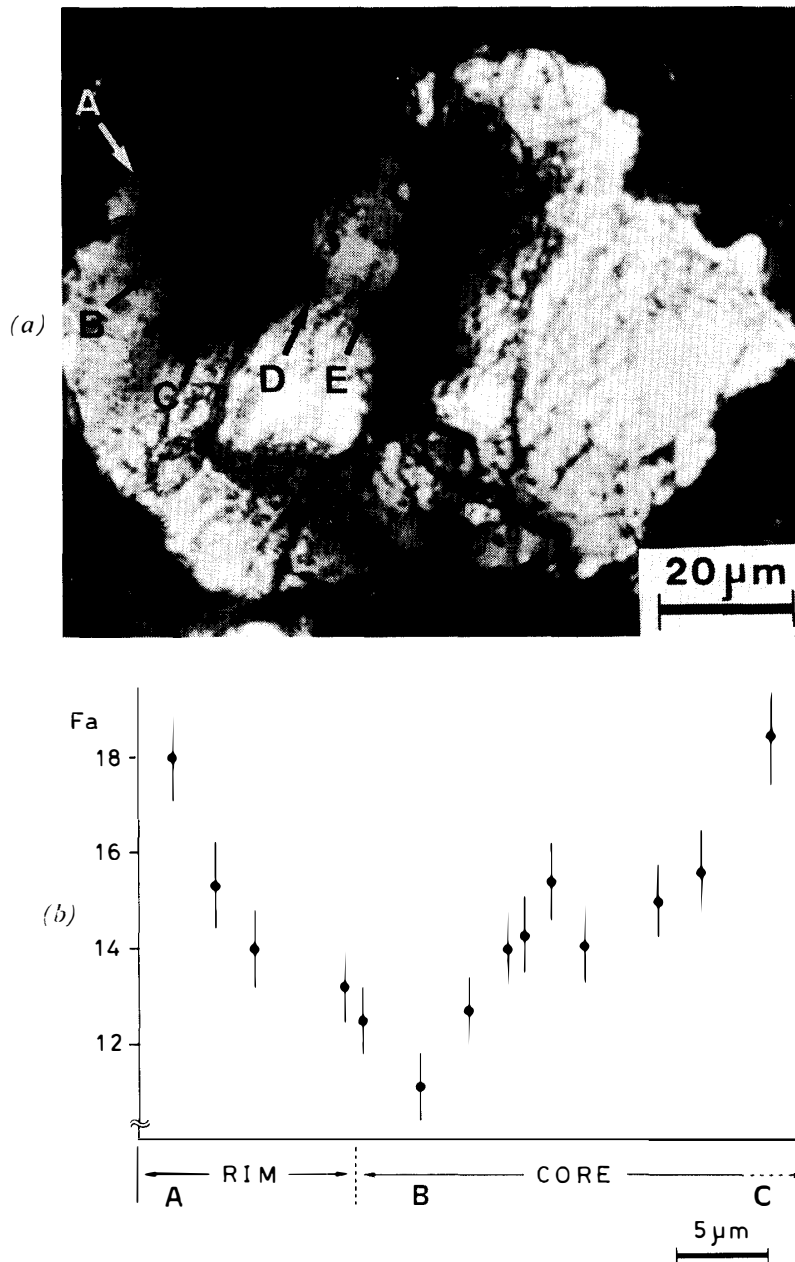


Fig. 2. (a) Optical micrograph of one of the relict olivine grains after ion-thinning. AEM analyses were made along A-B-C-D and at E. Crossed polarization. (b) Analytical results from A to C in (a).

sition of chromite but contains some effect from olivine around it. Other finer grains are too small for quantitative analyses but were identified to be chromite by containing Cr. Diffraction patterns show that chromite grains are not in a topotactic relation with olivine. Fe-metal inclusions were rarely found.

Figure 4 is a dark-field electron micrograph ($g=222$) near the boundary between the core and the rim of an olivine. Their dislocation densities were counted from the electron micrographs of the area where chromite and holes were not observed. As shown in Fig. 4, dislocations in the core are ubiquitous and show little rearrangement.

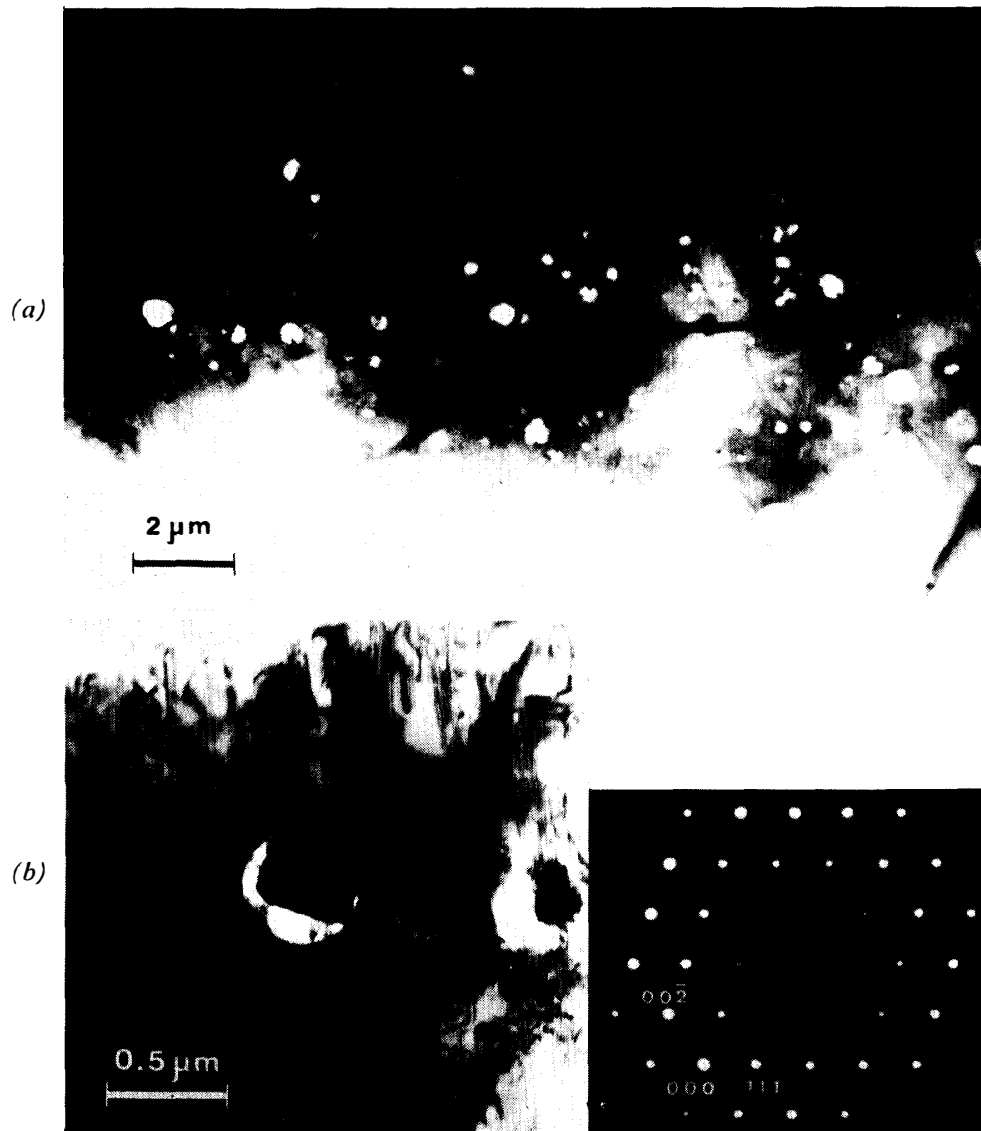


Fig. 3. (a) Electron micrograph of the dusty core of olivine. Chromite inclusions and ion-thinned holes around them are abundant. (b) Electron micrograph of chromite and diffraction pattern from it, which shows (111) twin.

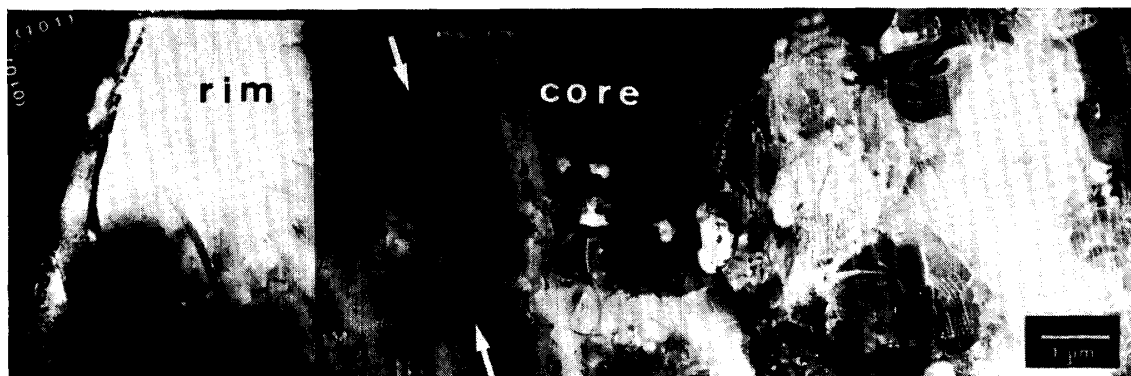


Fig. 4. Dark-field electron micrograph taken by $g=222$. The dislocation density is much higher in the core than the rim.

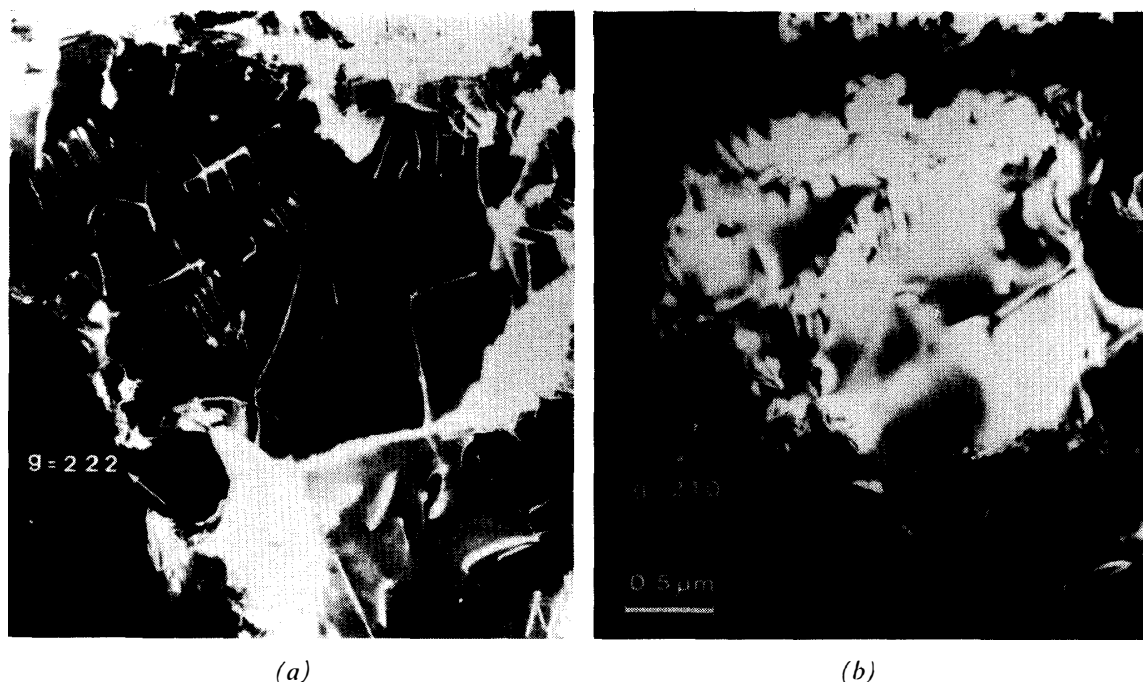


Fig. 5. (a) Dark-field electron micrograph ($g=222$) of the core. (b) Dark-field electron micrograph ($g=210$) of the same area as (a). Dislocations are now out of contrast.

The dislocation density of the core ($\sim 10^9/\text{cm}^2$) is extremely higher than that of the rim ($\sim 2 \times 10^8/\text{cm}^2$). In order to determine the Burgers vector of the dislocations, two-beam experiments of transmission electron microscopy were made. Figures 5a and 5b are dark-field electron micrographs of the same area taken by $g=222$ and 210, respectively.

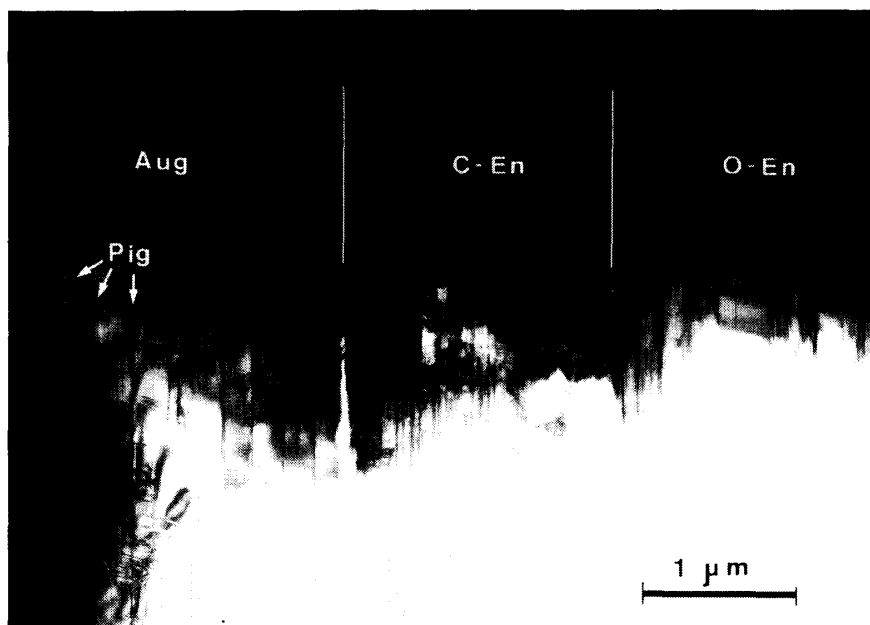


Fig. 6. Electron micrograph of pyroxene. Center of the grain is on the right side of the figure. Orthoenstatite (O-En) is mantled by clinoenstatite (C-En), which is rimmed by augite (Aug) with pigeonite lamellae (Pig).

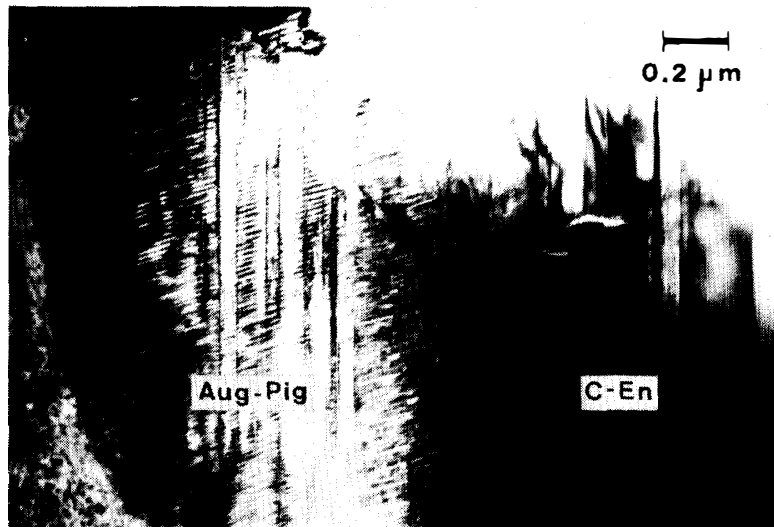


Fig. 7. Spinodal decomposition texture of augite and pigeonite. On the right side of the figure is clinoenstatite.

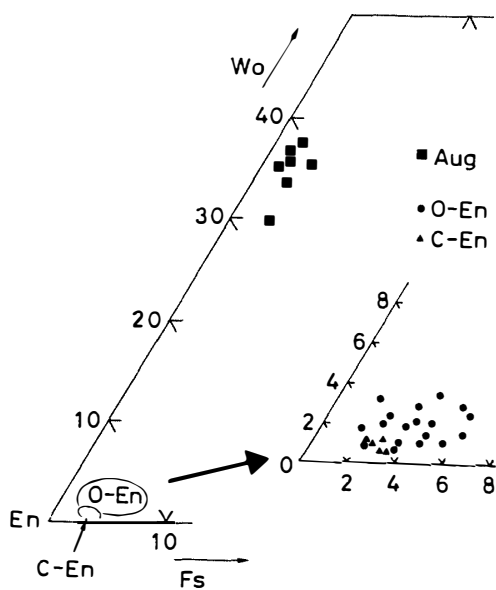


Fig. 8. Chemical composition of pyroxenes plotted on the pyroxene quadrilateral.

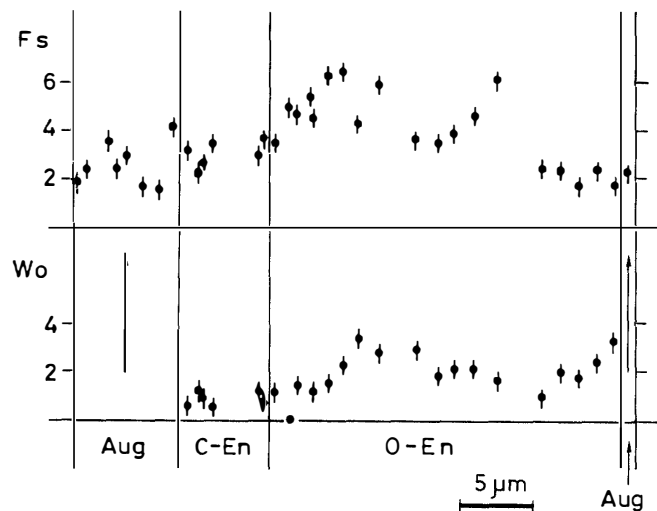


Fig. 9. Variations in Fs and Wo components across the pyroxene grain. In orthoenstatite, both components are richer than in clinoenstatite and, though the variations are not systematically, they tend to increase toward the central portion.

The dislocations are in and out of contrast in Figs. 5a and 5b, respectively, indicating that the Burgers vector of the dislocations is perpendicular to $[210]$. In this area, dislocations are also out of contrast for $g=040$. Thus, the Burgers vector, b , is $[001]$. A grain viewed along the c -axis shows dislocations in long straight segments aligned parallel to $[100]$ or $[010]$. In the two-beam experiments, the $[100]$ segments have weak contrast for $g=040$ and 100 . Though the Burgers vector cannot be uniquely determined only by these experiments, the Burgers vectors of olivine predicted from the crystal structure are $[001]$ and $[100]$ (CARTER and AVE' LALLEMENT, 1970). The $[100]$ segments

are therefore considered to be [001] edge dislocations. Because the [010] segments have clear and weak contrast for $g=400$ and 040 , respectively, they are considered to be [100] edge dislocations. In another grain viewed along $[\bar{1} 1 2]$, the dislocation lines parallel to the trace of the c -axis were in and out of contrast for $g=021$ and 110 , respectively, and are considered to be [001] screw dislocations. As a whole, [001] dislocations are much more predominant than [100] ones.

2.2. Pyroxene

Pyroxene grains consist of three parts: the orthoenstatite core is mantled by clinoenstatite and the outermost rim is augite (Figs. 6 and 7). Chemical compositions of pyroxenes are plotted in the pyroxene quadrilateral (Fig. 8) and listed in Appendix. Orthoenstatite is in the range of $\text{En}_{90-96}\text{Wo}_{1-4}\text{Fs}_{2-6}$, in which the central part is slightly richer in Fe and Ca than near the clinoenstatite (Fig. 9). Clinoenstatite is homogeneous, $\text{En}_{95-96}\text{Wo}_1\text{Fs}_{3-4}$. Augite is in the range $\text{En}_{60-67}\text{Wo}_{30-38}\text{Fs}_{2-4}$. Narrow Ca-poor parts of augite near clinoenstatite shows the spinodal decomposition texture of augite and pigeonite (Figs. 6 and 7), and Ca-rich part contains heterogeneous lamellae of pigeonite with the periodicity of ~ 20 nm (Fig. 6), though the AEM analyses do not resolve the host and lamellae.

3. Discussion

3.1. Olivine

AEM analysis of olivine shows the reverse and normal Fe-Mg zoning in the core and the rim, respectively. This is consistent with the previous results by NAGAHARA (1981a, b) and RAMBALDI (1981), and supports the conclusion that the dusty core of olivine is relict.

Furthermore, the higher dislocation density of the dusty core than the rim suggests that the preexisting olivine has experienced either i) severe shearing in a grand-parent body, or ii) intensive shock deformation. The typical terrestrial olivine derived from the upper mantle has the dislocation density of 10^7 – $10^8/\text{cm}^2$ with the predominance of the [100] dislocations (GREEN and RADCLIFFE, 1972), but the severe shearing as to result in the dislocation density of $10^9/\text{cm}^2$ is not likely in the grand-parent body of chondrites, which must not have highly differentiated. On the other hand, shock experiments on forsterite (MORI *et al.*, 1982) resulted in the predominant [001] screw dislocations of more than $10^9/\text{cm}^2$ dislocation density. Thus some shock impact is considered to be responsible for the dislocation structure of the core. ASHWORTH and BARBER (1975) studied the dislocation structure of olivine in some shock deformed meteorites and observed the [001] dislocation density of 10^8 – $10^9/\text{cm}^2$. Little annealing effect on the dislocations in the dusty core also supports preferentially the shock deformation to the shearing.

The rim of olivine also has a higher dislocation density ($\sim 2 \times 10^8/\text{cm}^2$) with the predominance of the [001] dislocations than that of the typical terrestrial olivine (10^7 – $10^8/\text{cm}^2$). This is explained by: i) shock impact after the formation of the chondrules, or ii) propagation of dislocations because of the overgrowth on the dusty core with the high dislocation density. The chondrules in the ALH-77015 chondrite have no evidence of shock, such as mosaicism of olivine, maskelynite and black veins, in pref-

erence of the second explanation. Therefore, the shock event must have either predated the melting process or taken place during the melting process. The duration of the melt stage at high temperatures must have been short enough to keep the dislocations with little rearrangement.

Fine chromite inclusions are abundant in the core of olivine, but are absent in the rim even in the electron microscopic scale. Therefore, they are considered to have either i) crystallized before the cores of olivine and been later included by it, or ii) initially resolved in the preexisting olivine and later precipitated or exsolved in it. Abundant distribution of small chromite grains throughout the dusty cores of olivine seems not compatible with the former process. The latter process, precipitation or exsolution, must have taken place before or during the formation of chondrules, because the dislocation structure of olivine and the decomposition texture of pyroxene indicate rapid cooling after solidification of them. Since chromite has no topotactic relation with olivine, precipitation in relation to partial melting is preferred to exsolution. RAMBALDI and WASSON (1982) reported that the inclusions in the dusty core are nickel-poor Fe metal and have possibly precipitated from olivine by its reduction during the formation of chondrules. The different inclusions, chromite and Fe-metal, may reflect difference in the initial composition of the preexisting olivine and in the redox state and pressure-temperature conditions before or during melting.

3.2. Pyroxene

Pyroxene grains in the radial pyroxene chondrules, which must once have been completely molten, show the crystallization sequence of clinoenstatite→pigeonite→augite in L3 chondrite (KITAMURA *et al.*, 1983) and orthoenstatite→pigeonite→augite in L4 and L5 (WATANABE *et al.*, 1985). These sequences are considered to reflect crystallization at rapid and slow cooling, respectively. However, the sequence in pyroxene in this chondrule, orthoenstatite→clinoenstatite→augite, cannot be explained by a single crystallization stage, since clinoenstatite generally crystallizes as protoenstatite at higher temperature than orthoenstatite. Chemical composition of orthoenstatite is heterogeneous but richer in Fe and Ca than that of clinoenstatite and is also incompatible with simple crystallization, similar to clinoenstatite which is considered to have been relict in the Allende chondrite (KITAMURA *et al.*, 1984). Therefore, the orthoenstatite is considered to be a relict crystal, like the dusty core of olivine.

4. Concluding Remarks

(1) The dusty cores of the relict olivine have a higher dislocation density ($\sim 10^9/\text{cm}^2$) than that of the rim ($\sim 2 \times 10^8/\text{cm}^2$). This high dislocation density and the predominance of [001] dislocations indicate that the dislocations have been caused by some shock impact before or during the melting process. Their little rearrangement also indicates that the olivine has not suffered long annealing after the shock event, even in the melting stage.

(2) Fine inclusions in the dusty core have been identified to be chromite.

(3) Apparent crystallization sequence of pyroxenes in this chondrule is orthoenstatite→clinoenstatite→augite. The orthoenstatite is considered to be relict, indi-

cating the preexistence of orthopyroxene in addition to olivine.

Acknowledgments

The authors thank Prof. T. NAGATA and Dr. K. YANAI of the National Institute of Polar Research for providing the samples.

References

- ASHWORTH, J. R. and BARBER, D. J. (1975): Electron petrography of shock-deformed olivine in stony meteorites. *Earth Planet. Sci. Lett.*, **27**, 43–50.
- CARTER, N. L. and AVE'LALLEMANT, H. G. (1970): High-temperature flow of dunite and peridotite. *Geol. Soc. Am. Bull.*, **81**, 2181–2202.
- FUJIMAKI, H., MATSU-URA, M., AOKI, K. and SUNAGAWA, I. (1981): Ferropseudobrookite—silica mineral—albite-chondrule in the ALH-77015 chondrite (L3). *Mem. Natl Inst. Polar Res., Spec. Issue*, **20**, 119–123.
- GREEN II, H. W. and RADCLIFFE, S. V. (1972): Deformation processes in the Upper Mantle. *Flow and Fracture of Rocks*, ed. by H. C. HEARD *et al.* Washington, D.C., Am. Geophys. Union, 139–156 (Geophys. Monogr. 16).
- KITAMURA, M., YASUDA, M., WATANABE, S. and MORIMOTO, N. (1983): Cooling history of pyroxene chondrules in the Yamato-74191 chondrite (L3)—An electron microscopic study. *Earth Planet. Sci. Lett.*, **63**, 189–201.
- KITAMURA, M., ISOBE, H., WATANABE, S. and MORIMOTO, N. (1984): Thermal history of 'relict pyroxene' in the Allende meteorite (abstract). Paper presented to the Ninth Symposium on Antarctic Meteorites, 22–24 March 1984. Tokyo, Natl Inst. Polar Res., 50–51.
- MORI, H., SHONO, Y., GOTO, T. and TAKEDA, H. (1982): Horusuteraito no shôgeki asshuku zanryû kôka no kôbutsugaku-teki kenkyû (Mineralogical study of remanent effect of shock compression on forsterite). *Nihon Kôbutsu Gakkai 1982-nen kai Kôen Yôshishû* (Mineralogical Society of Japan, 1982 Annual Meeting Abstracts with Programs), 66.
- MORIMOTO, N. and KITAMURA, M. (1981): Application of 200 kV analytical electron microscopy to the study of fine textures of minerals. *Bull. Minéral.*, **104**, 241–245.
- NAGAHARA, H. (1981a): Evidence for secondary origin of chondrules. *Nature*, **292**, 135–136.
- NAGAHARA, H. (1981b): Petrology of chondrules in ALH-77015 (L3) chondrite. *Mem. Natl Inst. Polar Res., Spec. Issue*, **20**, 145–160.
- RAMBALDI, E. R. (1981): Relict grains in chondrules. *Nature*, **293**, 558–561.
- RAMBALDI, E. R. and WASSON, J. T. (1982): Fine, nickel-poor Fe-Ni grains in the olvine of unequilibrium ordinary chondrites. *Geochim. Cosmochim. Acta*, **46**, 929–939.
- WATANABE, S., KITAMURA, M. and MORIMOTO, N. (1985): A transmission electron microscope study of pyroxene chondrules in equilibrated L-group chondrites. *Earth Planet. Sci. Lett.*, **72**, 87–98.

(Received June 4, 1984; Revised manuscript received July 25, 1984)

Appendix. Number of cations by AEM.*

	Si	Ti	Al	Cr	Fe	Mg	Ca	Total
Ol**	0.99	—	—	—	0.36	1.66	—	3.01
Ol	0.97	—	—	—	0.32	1.74	—	3.03
Ol	0.98	—	—	—	0.28	1.75	—	3.01
Ol	0.99	—	—	—	0.27	1.75	—	3.01
Ol	0.98	—	—	—	0.26	1.79	—	3.03
Ol	1.00	—	—	—	0.22	1.79	—	3.01
Ol	1.00	—	—	—	0.25	1.74	—	2.99
Ol	1.01	—	—	—	0.28	1.71	—	3.00
Ol	1.00	—	—	—	0.29	1.72	—	3.01
Ol	0.99	—	—	—	0.31	1.70	—	3.00
Ol	1.00	—	—	—	0.28	1.72	—	3.00
Ol	1.00	—	—	—	0.30	1.69	—	2.99
Ol	1.00	—	—	—	0.31	1.69	—	3.00
Ol	1.01	—	—	—	0.37	1.61	—	2.99
Chromite	0.45	—	0.06	1.15	0.66	0.63	—	2.95
Aug***	1.90	0.04	0.18	0.03	0.03	1.09	0.67	3.94
Aug	1.91	0.03	0.19	0.03	0.04	1.08	0.67	3.95
Aug	2.00	0.01	0.11	0.02	0.06	1.19	0.53	3.92
Aug	1.95	0.04	0.19	0.03	0.04	1.05	0.60	3.90
Aug	1.96	0.02	0.20	0.02	0.05	1.09	0.57	3.91
Aug	1.95	0.02	0.20	0.02	0.03	1.07	0.64	3.93
Aug	1.95	0.02	0.17	0.03	0.03	1.12	0.62	3.94
Aug	1.91	0.02	0.16	0.02	0.08	1.13	0.66	3.98
C-En	1.96	0.00	0.10	0.01	0.06	1.84	0.01	3.98
C-En	1.86	—	0.08	0.02	0.04	1.86	0.02	3.98
C-En	1.99	0.01	0.06	0.01	0.05	1.82	0.02	3.96
C-En	2.00	0.01	0.09	0.02	0.06	1.74	0.01	3.93
C-En	1.99	—	0.08	0.02	0.06	1.79	0.02	3.96
C-En	1.93	0.01	0.07	0.03	0.07	1.89	0.01	4.01
O-En	1.99	0.01	0.06	0.02	0.07	1.79	0.02	3.96
O-En	1.99	0.01	0.08	0.02	0.09	1.76	0.00	3.95
O-En	2.00	—	0.07	0.02	0.09	1.74	0.03	3.95
O-En	2.01	—	0.08	0.03	0.08	1.73	0.02	3.95
O-En	1.96	0.00	0.08	0.02	0.10	1.79	0.02	3.97
O-En	1.99	0.00	0.07	0.02	0.12	1.73	0.03	3.96
O-En	1.99	0.01	0.11	0.03	0.12	1.62	0.04	3.92
O-En	1.96	0.00	0.11	0.04	0.08	1.70	0.06	3.95
O-En	1.93	0.00	0.11	0.03	0.11	1.75	0.05	3.98
O-En	1.91	0.01	0.12	0.04	0.07	1.78	0.06	3.99
O-En	1.91	0.01	0.10	0.05	0.07	1.80	0.03	3.97
O-En	1.97	0.01	0.11	0.06	0.07	1.69	0.04	3.95
O-En	1.94	—	0.13	0.05	0.09	1.72	0.04	3.97
O-En	1.95	0.01	0.08	0.03	0.12	1.77	0.03	3.99
O-En	1.97	0.00	0.10	0.02	0.04	1.82	0.02	3.97
O-En	1.93	—	0.10	0.01	0.05	1.89	0.04	4.02
O-En	1.92	0.01	0.11	0.03	0.03	1.85	0.03	3.98
O-En	2.00	0.01	0.10	0.02	0.04	1.70	0.04	3.91
O-En	1.92	0.00	0.18	0.01	0.03	1.77	0.06	3.97
Aug	1.97	0.03	0.13	0.02	0.04	1.10	0.63	3.92

*Numbers of oxygen are 4 for olivine and chromite and 6 for pyroxenes, respectively.

**Analytical points of olivine correspond to those from left to right of Fig. 2b.

***Analytical points of pyroxenes correspond to those from left to right of Fig. 9.